Sparse 3D Radon Space Rigid Registration of CT Scans: Method and Validation Study

G. Medan, N. Shamul, and L. Joskowicz,* *Fellow, IEEE*

***Abstract*— We present a new method for rigid registration of CT datasets in 3D Radon space based on sparse sampling of scanning projections. The inputs are the two 3D Radon transforms of the CT scans, one densely sampled and the other sparsely sampled (limited number of scan angles/ranges). The output is the rigid transformation that best matches them. The method first finds the best matching between each projection direction vector in the sparse transform and the corresponding direction vector in the dense transform. It then solves a system of linear equations derived from the direction vector pairs (parallel-beam projections) or finds a solution by non-linear optimization (fan-beam and cone-beam projections). Experimental studies show that our method for 3D parallel beam registration outperforms image space registration in terms of convergence range with significantly reduced X-ray dose compared to a full conventional CT scan.**

***Index Terms*— CT scanning, image processing, Radon transform, reduced-dose scanning, rigid registration.**

I. Introduction

RIGID registration of CT scans and/or CT data acquired at different times plays a key role in numerous medical applications, including diagnosis, follow-up, treatment planning, and interventional CT. Rigid registration methods, including fiducial, intensity, and frequency-based methods are nowadays common in clinical use in diagnostic, interventional radiology and radiotherapy.

Rigid registration of CT scans and/or CT projection data is an important first step for non-rigid registration, in which the scanned structures may be displaced as a result of different patient poses and soft tissue deformations, e.g., breathing. In these cases, rigid registration is used to bring the datasets into coarse correspondence, which is then refined by computing the deformations field to establish the fine correspondence.

Rigid registration of a CT scan to the patient is a prerequisite in radiotherapy and radiosurgery, where the preoperative CT scan on which radiation plan was designed is aligned with the patient pose prior to treatment. Registration also plays an important role in image-guided interventional CT (ICT) procedures, e.g., biopsies, catheter insertion, and hematoma evacuation. Often times, a high-quality CT scan of the patient is available either before the procedure or at the beginning of it. Since the procedure planning is performed on this CT scan, it is desirable to use it for guidance during the intervention. To monitor the progress of the surgery, evaluate anatomical changes, and determine the surgical tools location, repeated CT scanning is often performed. This results in the exposure of the patient to cumulative ionizing radiation, which has been shown to have risks for the patient and the crew [1], [2]. It is thus highly desirable to develop methods to reduce the radiation dose required for intraoperative CT registration.

Manuscript received July 31, 2016; revised September 28, 2016; accepted October 1, 2016. Date of publication October 6, 2016; date of current version February 1, 2017. Research supported by Kamin Grant 52643, Office of the Chief Scientist, Ministry of Trade and Industry, Israel. We thank Eyal Lin and Ronen Shter of GE Healthcare Israel for the CT scans and for their valuable assistance. *Asterisk indicates corresponding author.*

G. Medan and N. Shamul are with the CASMIP Laboratory, School of Computer Science and Engineering, The Hebrew University of Jerusalem, Jerusalem 91904, Israel.

*L. Joskowicz is with the CASMIP Laboratory, School of Computer Science and Engineering, The Hebrew University of Jerusalem, Jerusalem 91904, Israel (e-mail: josko@cs.huji.ac.il).

Digital Object Identifier 10.1109/TMI.2016.2615653

II. Related Work

The main approaches for rigid registration of patients/CT scans are: 1) point-based, 2) image-based CT to CT, 3) image-based X-ray to CT, and 4) Radon-based registration.

Point-based methods compute the rigid transformation by matching points defined in CT scans and minimizing the sum of their pairwise distances [3]. Since these methods require the explicit identification and matching of points, their scope is limited to selected clinical scenarios.

Image-based CT to CT methods perform the registration by comparing the intensity values of both CT images [4]. To yield adequate results, they require both CT scans to be of good quality, be free of image reconstruction artifacts, and have small scanned subject/pose discrepancies. Recently, cone-beam CT imaging devices were introduced for radiation therapy and interventional radiology. They support image-based patient and CT registration with a radiation dose of 1/3-1/2 of that of a standard CT scanner [5]. Consequently, only a few repeat CT scans can be acquired during the procedure.

Numerous image-based 2D X-ray to 3D CT registration methods have been developed [6]–[8]. Some are in routine clinical use for image-guided therapy and for patient positioning during treatment (see [6] for a comprehensive survey). In all cases, the matching procedure requires at least two (and often more) X-ray images of sufficient quality for the matching. The drawbacks of these methods are that they may use different hardware for CT and X-ray acquisition, that they require set-up time, and that they cannot reduce the radiation dose below that of the X-ray image acquisition.

Radon-space methods, also called sinogram or projection-space methods, use the CT scans Radon transform

0278-0062 © 2016 IEEE. Personal use is permitted, but republication/redistribution requires IEEE permission.
See http://www.ieee.org/publications_standards/publications/rights/index.html for more information.

representation (sinograms) for the registration. They do not suffer from image reconstruction artifacts and have the potential to yield robust and accurate results with greatly reduced doses.

Previous research addresses rigid registration in Radon space [8]–[15]. Freiman et al. [9] describe a 2D/3D registration method for X-ray to CT scans that uses invariant Fourier space features to find the transformation parameters by out-of-plane coarse registration followed by in-plane fine registration. Mao et al. [10] describe a slice-by-slice registration method in 2D Radon space and its extension to 3D for small angles. Mooser et al. [11] propose an iterative optimization method to compute the registration parameters in 3D Radon space for full scans. You et al. [12] investigate the invariant properties of rigid movement in image and Radon space. Based on this work, Lu, Fitchard et al. [13]–[15] use Fourier phase matching to iteratively compute the rigid registration parameters by decomposing the 3D problem into a series of 2D in-plane registrations. The method is limited to small transformations.

More recently, Wein et al. [16], Aichert et al. [17], [18], and Debbler et al [31] use directed epipolar geometry to establish consistency metrics between different projection views for the detection of mid-scan patient motion. However, their methods do not address inter-scan registration. The 2D Radon transform was shown to be very useful for pattern matching and registration of 2D images, both in terms of accuracy, convergence range and noise robustness [29], [30]. However, the authors do not indicate how their methods can be extended to 3D and to real sinogram data.

Deformable registration in projection space methods are described in [19], [20]. Osorio et al. [19] describe a Fourier space based on full CT scans. Zhang et al. [20] present a method that iteratively matches the repeat scan projection to the re-projected deformed baseline. The method requires a preceding rigid registration step to allow convergence of the deformation field to the optimal solution.

Large reductions in radiation dose have been shown for 3D/2D registration between CT and C-arm fluoroscopy [21]. Very recently, ultralow-dose CT scanning became available in commercial systems. While the resulting images have been shown to be clinically useful in several tasks, it has yet to be determined if they can be used for repeated intra-operative patient to CT registration.

In summary, the main drawbacks of the existing methods are: 1) a significant part of the repeat CT projection data is required, thus limiting the feasible radiation dose reduction; 2) limited range of convergence; 3) iterative solutions with long computation times, and; 4) lack of comprehensive accuracy and convergence studies. Moreover, previous works do not explicitly address the problem of rigid registration with very low-dose CT scans [22].

III. Method

In [24] we describe a new method for rigid registration CT scans and/or registration of a patient to his/her baseline CT scan in 3D Radon space using sparse scanning projections sampling. The inputs are the two 3D Radon transforms of the CT scans, one densely sampled in the projections view domain, and the other sparsely sampled. The output is the rigid transformation that best matches the 3D Radon transforms. The algorithm computes for each direction vector in the sparse 3D Radon transform the best matching direction vector in the dense 3D Radon transform. It then solves a system of linear equations derived from the direction vector pairs (parallel-beam projections [24]), or performs non-linear optimization (fan- and cone-beam projections).

The advantages of our method are: 1) it can be used both to register two CT scans and to register a baseline scan to the patient with ultra-low dose scanning without compromising registration accuracy; 2) it supports repeated on-line patient-to-baseline CT scan registration without significant increase of the radiation dose; 3) it has a wide convergence range.

A. Background

In [24] we showed that for images $f, g : \mathbb{R}^3 \to \mathbb{R}$ related by a rigid transformation $g(X) = f(A_{\boldsymbol{r},\theta}X+X_0)$ (where $X_0 \in R^k$ is a translation, and $A_{\boldsymbol{r},\theta}$is a rotation matrix representing a rotation of angle θ about axis $\boldsymbol{r}$), the rigid registration parameters can be recovered by a process of matching their 3D Radon transforms $\boldsymbol{\mathcal{R}}$, defined by:

$$F_{\boldsymbol{n}}(s) = \boldsymbol{\mathcal{R}} f(\boldsymbol{n}, s) \int_{H(\boldsymbol{n},s)} f(X) d\mu \tag{1}$$

where $H(\boldsymbol{n}, s)$ is the plane defined by normal vector $\boldsymbol{n}$ and signed distance from the origin s, and $d\mu$ is the standard measure on the plane.

The algorithm is based on the following relation between F and G:

$$G_{\boldsymbol{n}}(s) = F_{\boldsymbol{n}'}(s - \boldsymbol{n}\cdot X_0) \tag{2}$$

where $\boldsymbol{n}$ and $\boldsymbol{n}'$ are normal unit direction vectors satisfying:

$$\boldsymbol{n} = A_{r,\theta}\boldsymbol{n}'. \tag{3}$$

In order to find the parameters of the rigid registration, we assume F and G are given for discrete sets of directions $\{\boldsymbol{n}_i\}$ associated with F and $\{\boldsymbol{n}'_j\}$ associated with G. We then find matches between them and record their relative s-offsets $\boldsymbol{\Delta}$: $F_{\boldsymbol{n}'}, G_{\boldsymbol{n}}$ are 1-dimensional signals in s, and the similarity (up to an offset in s)$G_{\boldsymbol{n}}(s) \cong F_{\boldsymbol{n}'}(s - \boldsymbol{\Delta}_i)$ implies that $\boldsymbol{n}', \boldsymbol{n}, \Delta$ are related by Eq. (3) and by $\Delta = \boldsymbol{n}\cdot X_0$. We construct a linear system of equations and solve using RANSAC for outlier removal to estimate $A_{r,\theta}$ and X_0. We chose the 1D Normalized Cross Correlation (NCC) function to provide a score for any given match $(F_{\boldsymbol{n}'}, G_{\boldsymbol{n}}, \Delta)$.

A key property of this method is that it does not require a dense set of direction vectors of the 3D Radon transform of the repeat scan g, a property which allows the radiation dose reduction of our algorithm. The details of the algorithm are summarized in Table I.

The computation of $\boldsymbol{\mathcal{R}}f$ and $\boldsymbol{\mathcal{R}}g$ is a key step in our method: it should not be done directly from the reconstructed f and g, since this would assume that the reconstructed g is available. As the repeat scan is performed with a limited set of projections, obtaining a valid reconstruction of g is not feasible unless the patient is exposed once more to a full scan dose, which is undesirable. Therefore, we propose a different

TABLE I
3D PPARALLEL-BEAM RADON SPACE REGISTRATION ALGORITHM

Input	• Densely sampled baseline scan, converted to 3D Radon: $F_{\boldsymbol{n}'_j}$ for a dense set of directions $\{\boldsymbol{n}'_j\}$. • Sparsely sampled repeat scan, converted to 3D Radon: $G_{\boldsymbol{n}_i}$ for a sparse set of directions $\{\boldsymbol{n}_i\}$.
	1. Match the directions to produce a pairing set $\{(\boldsymbol{n}'_{j(i)}, \boldsymbol{n}_i, \Delta_i)\}$ where: $(j(i), \Delta_i) = \underset{j,\Delta}{\operatorname{argmax}}\, NCC\left(F_{\boldsymbol{n}'_j}(s-\Delta), G_{\boldsymbol{n}_i}(s)\right)$ such that: $G_{\boldsymbol{n}_i}(s) \cong F_{\boldsymbol{n}'_{j(i)}}(s-\Delta_i)$ 2. Compute the rigid registration parameters: a. Solve for $\boldsymbol{X_0}$: $\{\Delta_i = \boldsymbol{n}_i \cdot X_0\}$ b. Solve for $A_{r,\theta}$: $\{\boldsymbol{n}_i = A_{r,\theta}\boldsymbol{n}'_{j(i)}\}$ c. Apply RANSAC to filter outliers.
Output	Rigid registration which best aligns f and g: $g(X) \cong f(A_{r,\theta}X + \boldsymbol{X}_0)$

approach to computing $\mathcal{R}g$ and $\mathcal{R}f$: work directly on the sinogram data from the CT scanner. This data is stack of 2D sinogram, one for each slice of the imaged volume, which we denote $\{\mathcal{R}_{2D}\{f_{Z=z}\}\}_{z=zmin}^{zmax}$.

Each sample value $F_{\boldsymbol{n}}(s)$ of $\mathcal{R}f$ represents a summation of f over a plane $H(\boldsymbol{n}, s)$ with normal $\boldsymbol{n}$ and distance s from the origin. This operation on f can be replaced by a summation of terms, each of which representing summation along parallel rays contained in the plane $H(\boldsymbol{n}, s)$. If we choose these rays such that each one is also contained in a slice of f (a plane f_Z parallel to the xy plane), then the term for each ray is given by the 2D Radon transform of the containing slice at the appropriate distance and orientation for each ray. Formally:

$$\mathcal{R}f(\boldsymbol{n}, s) = \int_{H(\boldsymbol{n},s)} f(X)\, d\mu \propto \int_z \mathcal{R}_{2D}\{f_{Z=z}\}(\theta(\boldsymbol{n}), t(s,z))dz. \quad (4)$$

This formulation is further simplified by considering the 3D dataset $\{\mathcal{R}_{2D}\{f_{Z=z}\}\}_{z=zmin}^{zmax}$ as a series of projection images $\{\boldsymbol{P}_{\boldsymbol{\theta}}(t,z)\}_{\theta=0^o}^{360^o}$ and using a second 2D Radon transform:

$$\mathcal{R}f(\boldsymbol{n}, s) \propto \mathcal{R}_{2D}\left\{\boldsymbol{P}_{\theta(\boldsymbol{n})}\right\}(\phi(\boldsymbol{n}), t(s,z)) \quad (5)$$

where $\theta(\boldsymbol{n}), \phi(\boldsymbol{n})$ are the spherical coordinates of the unit vector $\boldsymbol{n}$. Thus, when the sinograms are given for a set $\theta \in \Theta$ of projection directions and the 2D Radon transforms of $\boldsymbol{P}_\theta$ are performed to obtain a set $\phi \in \Phi$ of projection directions, the resulting set of direction vectors is $\{\boldsymbol{n} : (\theta(\boldsymbol{n}), \phi(\boldsymbol{n})) \in \Theta \times \Phi\}$.

In this manner, the 3D Radon signals $\mathcal{R}f(\boldsymbol{n}, s), \mathcal{R}g(\boldsymbol{n}, s)$ are computed without requiring the images f and g to be available, only their slice-wise 2D sparse Radon transforms. Table I summarizes the method.

B. 2D Fan-beam registration

In 2D fan-beam scanning geometry, a single ray is parameterized by (ϕ, γ), where ϕ is the view angle of the X-ray source position and γ is the detector fan angles relative to the central ray through the origin (Fig. 1). The fan-beam transform

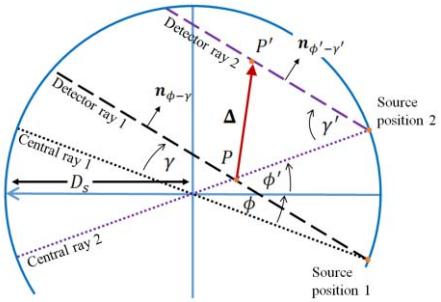

Fig. 1. Fan-beam geometry: rigid translation without rotation. Detector ray 1 passing through point P is seen from view angle ϕ (Source position 1) at detector angle γ relative to Center ray 1. For a rigid translation of P by Δ to P', the ray retains its global orientation $\boldsymbol{n}_{\phi-\gamma}$, resulting in view angle change (Source position 2) and detector angle relative to Central ray 2 to (ϕ', γ'). The normals to Detector rays 1 and 2 are identical, $\boldsymbol{n}_{\phi-\gamma} = \boldsymbol{n}_{\phi'-\gamma'}$. The detector ray distances from the origin are $D_s sin\gamma$, $D_s sin\gamma'$, where D_S is the distance between the source and the coordinates origin.

is defined as the line integral:

$$\mathcal{R}^{FB}\{f\}(\phi, \gamma) = \int_{L(\phi,\gamma)} f(X)\, dl \quad (6)$$

where $L(\phi, \gamma)$ is the line and dl is the line infinitesimal. The line $L(\phi, \gamma)$ is defined by $X | X \cdot \boldsymbol{n}_{\phi-\gamma} = D_s \sin\gamma\}$ where D_s is the source-to-origin distance and $\boldsymbol{n}_{\phi-\gamma}$ is the unit normal to the detector ray and $\boldsymbol{n}_\alpha = (\cos\alpha, \sin\alpha)$.

The goal is to find how a rigid transformation $\mathcal{T}_{\varphi,\boldsymbol{\Delta}}$ in 2D space affects the fan-beam transform of an object, where φ is its rotation about the origin, and $\boldsymbol{\Delta}$ is its translation. We seek the transformation $\tilde{\mathcal{T}}_{\varphi,\boldsymbol{\Delta}} : (\phi, \gamma) \rightarrow (\phi', \gamma')$ that relates the fan-beam transform of object $\mathcal{R}^{FB}\{f\}$ to its Radon transform:

$$\mathcal{R}^{FB}\left\{T_{\varphi,\boldsymbol{\Delta}}\{f\}\right\} = \tilde{\mathcal{T}}_{\varphi,\boldsymbol{\Delta}}\left\{\mathcal{R}^{FB}\{f\}\right\}. \quad (7)$$

To find $\tilde{\mathcal{T}}_{\varphi,\boldsymbol{\Delta}}$, consider the relation between the 2D parallel beam representation of a ray and its fan-beam representation $(\theta, r)^{PB} \sim (\phi', \gamma')^{FB}$:

$$\theta = \phi - \gamma \text{ and } r = D_s \sin\gamma. \quad (8)$$

From the known relations of the 2D parallel-beam registration we derive that:

$$\theta' = \theta + \varphi \text{ and } r' = r + \boldsymbol{n}_\theta \cdot \boldsymbol{\Delta}. \quad (9)$$

For 2D translation with no rotation, by (8), (9) with $\varphi = 0$:

$$\phi' - \gamma' = \phi - \gamma \text{ and } D_s \sin\gamma' = D_s \sin\gamma + \boldsymbol{n}_{\phi-\gamma} \cdot \boldsymbol{\Delta}. \quad (10)$$

For 2D rotation and translation, a global rotation φ is added to the orientation of the ray. Thus, by (10):

$$\phi' - \gamma' = \phi - \gamma + \varphi. \quad (11)$$

Sparse sampling of viewing directions in fan-beam geometry results in a parallel-beam representation which is composed of sinusoidal curves in $(\theta, r)^{PB}$ plane (Eq. 8). This property makes it difficult to extend the parallel-beam algorithm as-is to this case, as each fan-beam detector ray corresponds to a different parallel-beam projection angle and therefore rigid movement affects its repeat-scan coordinates slightly differently.

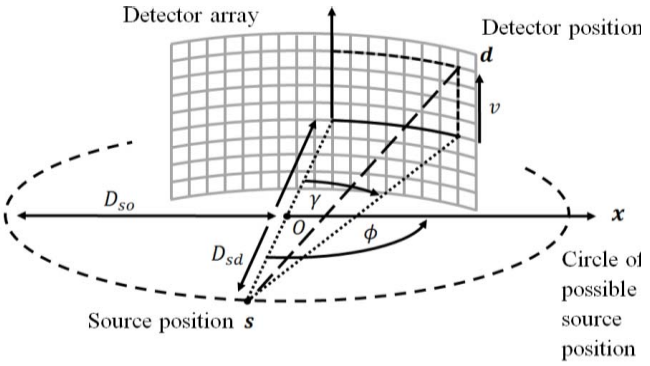

Fig. 2. Cone-beam scanning geometry. The origin and center of the source positions circle is O, and the source and detector origin positions are s,d. The detector ray (dashed line) is described by (ϕ, γ, v), where ϕ is the angle between the x axis and source position s, γ is the angle in the xy plane between the lines *sO* and the projection of *sd*, and *v* is the vertical detector offset.

We therefore adapt the above equations for use in an iterative cost-function minimization context.

We define next a cost function for fan-beam similarity. Let scans $\mathcal{R}^{FB}\{f\}(\phi,\gamma)$ and $\mathcal{R}^{FB}\{g\}(\phi,\gamma)$ be two scans with view angles/source positions $\phi \in \{\phi_1,\ldots,\phi_K\}$ where f and g are related by an unknown rigid transformation $T_{\varphi,\boldsymbol{\Delta}}$. Then:

$$C(\varphi,\boldsymbol{\Delta}) = \sum_{i=1}^{K} \log\left(1 - NCC\left[\tilde{\mathcal{T}}_{\varphi,\boldsymbol{\Delta}}\left\{\mathcal{R}^{FB}\{f\}\right\}(\phi_i,\cdot), \mathcal{R}^{FB}\{g\}(\phi_i,\cdot)\right]\right) \quad (12)$$

where NCC is the 1D NCC function, $\mathcal{R}^{FB}\{g\}(\phi_i,\cdot)$ is the 1D signal along the detector arc in a single view angle for scan g. When it is similar to the same signal from $\mathcal{R}^{FB}\{f\}$ under a given rigid transformation by $\varphi, \boldsymbol{\Delta}$ with transformation $\tilde{\mathcal{T}}_{\varphi,\boldsymbol{\Delta}}$, the cross-correlation is high and the cost is low.

Fan-beam rigid registration is computed iteratively. It starts from an initial guess and moves in 3D parameter space towards a solution with a lower cost until a local optimum is found, i.e., when all views of $\mathcal{R}^{FB}\{g\}$ have a high cross-correlation similarity with the resulting $\tilde{\mathcal{T}}_{\varphi,\boldsymbol{\Delta}}\{\mathcal{R}^{FB}\{f\}\}$.

The fan-beam rigid registration algorithm inputs a sparse scan $\mathcal{R}^{FB}\{g\}$), a dense scan $\mathcal{R}^{FB}\{f\}$, and an initial guess. The sampling of $\mathcal{R}^{FB}\{f\}$ is dense in viewing angles so that the interpolation of its values with transformation $\tilde{\mathcal{T}}_{\varphi,\boldsymbol{\Delta}}$ provides sufficiently accurate values for estimating the correlation with $\mathcal{R}^{FB}\{g\}$. The transformation parameters are computed by minimizing C over the 3D space of $(\varphi,\boldsymbol{\Delta})$ using derivative-free optimization methods such as downhill simplex:

$$\left(\hat{\varphi},\hat{\boldsymbol{\Delta}}\right) = \min_{\varphi,\boldsymbol{\Delta}} C(\varphi,\boldsymbol{\Delta}). \quad (13)$$

C. Cone-beam registration

In cone-beam CT acquisition, the X-ray source moves along a circle of radius D_{so}. The detectors are arranged as an array on a cylinder of radius D_{sd} centered at the source and oriented parallel to the z axis (Fig. 2). The 3D cone-beam transform is:

$$\mathcal{R}^{CB}\{f\}(\phi,\gamma,\upsilon) = \int_{L(\phi,\gamma,\upsilon)} f(X)dl \quad (14)$$

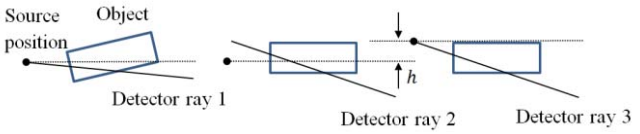

Fig. 3. Simplified side view scenario of cone-beam geometry scanning: (left) an object (rectangle) and ray path (Detector ray 1) originate at the X-ray source (dot); the dotted line is the source plane of rotation; (center) when the object is rotated with respect to the source, Detector ray 2 no longer intersects the circle traversed by the source - therefore information is missing about the ray's reading in the object's cone-beam transform; (right) the source plane of rotation is virtually shifted by *h* so that Detector ray 3 originates at the source. Since the path integrals along Detector rays 1 and 3 are identical, so are the detector readings corresponding to each ray. The reading from Detector ray 3 can be used to predict the reading of Detector ray 1 for the given rotation.

where $L(\phi,\gamma,\upsilon)$ is the line and dl is the line infinitesimal, ϕ is the viewing angle defining the source position, γ is the fan angle in the axial plane, and υ is the detector offset in the z direction. The line $L(\phi,\gamma,\upsilon)$ is between the source position $\boldsymbol{s}$ and the detector position $\boldsymbol{d}$, each defined as:

$$\boldsymbol{s} = \begin{bmatrix} -D_{so}\cos\phi \\ -D_{so}\sin\phi \\ h \end{bmatrix} \text{ and } \mathbf{d} = \boldsymbol{s} + \begin{bmatrix} D_{sd}\cos(\phi-\gamma) \\ D_{sd}\sin(\phi-\gamma) \\ \upsilon \end{bmatrix}. \quad (15)$$

We extend the fan-beam formulation to 3D cone-beam in Radon space as follows. Let $f, g : \mathbb{R}^3 \to \mathbb{R}$ be two scans related by a rigid transformation $T_{r,\theta,\boldsymbol{\Delta}}$ for rotation axis r, rotation angle θ, and translation $\boldsymbol{\Delta}$ so that $T_{r,\theta,\boldsymbol{\Delta}}\{f\} = g$. The goal is to find the transformation $\tilde{\mathcal{T}}^{CB}_{r,\theta,\boldsymbol{\Delta}}$ such that:

$$\tilde{\mathcal{T}}^{CB}_{r,\theta,\boldsymbol{\Delta}}\left\{\mathcal{R}^{CB}\{f\}\right\} = \mathcal{R}^{CB}\{g\}. \quad (16)$$

In 3D, not all the relevant projection information is available in $\mathcal{R}^{CB}\{f\}$: transformations that are pure z axis rotations or pure xy plane translationswill have no missing information. However, general transformations yield a transformation $\mathcal{R}^{CB}\{g\}$ where almost all detectors correspond to ray paths through the object which are not recorded by $\mathcal{R}^{CB}\{f\}$ since the rays emanating from the X-ray source traverse a planar circle and the transformed ray paths do not intersect it (Fig. 3).

To address this, we add a parameter h to describe the shift of the source in the z direction.The new cone-beam transform is:

$$\mathcal{R}^{CB*}\{f\}(\phi,\gamma,\upsilon,h) = \int_{L(\phi,\gamma,\upsilon,h)} f(X)dl \quad (17)$$

where the source traverses a planar circle in a virtual source plane that is parallel to the original source plane at signed-source position $\boldsymbol{s} = (D_{so}cos\phi, D_{so}\sin\phi, h)$ and detector position $\boldsymbol{d} = \boldsymbol{s} + (D_{sd}\cos(\phi-\gamma), D_{sd}sin(\phi-\gamma), \upsilon)$. The source positions circle then becomes a cylinder:

$$\mathcal{R}^{CB}\{f\}(\phi,\gamma,\upsilon) = \mathcal{R}^{CB*}\{f\}(\phi,\gamma,\upsilon,h=0). \quad (18)$$

The extended 3D cone-beam transform can be computed offline via a forward cone-beam projection of the reconstructed f. The projection space transformation $\tilde{\mathcal{T}}^{CB}_{r,\theta,\boldsymbol{\Delta}}$ is:

$$\tilde{\mathcal{T}}^{CB}_{r,\theta,\boldsymbol{\Delta}}\left\{\mathcal{R}^{CB*}\{f\}\right\} = \mathcal{R}^{CB}\{g\}. \quad (19)$$

We obtain $\tilde{\mathcal{T}}_{r,\theta,\mathbf{\Delta}}$ as follows. Let $\mathbf{s}, \mathbf{d}$ be the source and detector positions for view angle ϕ, source virtual offset h, and detector coordinates γ, υ. We parameterize the ray between the source and detector transformed by $T_{r,\theta,\mathbf{\Delta}}$ as:

$$\boldsymbol{q}(t) = T_{r,\theta,\mathbf{\Delta}}[\boldsymbol{s} + t(\boldsymbol{d} - \boldsymbol{s})]. \tag{20}$$

for $0 \leq t \leq 1$. This ray intersects the cylinder of source positions when $t = t_{so}$:

$$t_{so} = \min\left\{t : q_x^2(t) + q_y^2(t) = D_{so}^2\right\}. \tag{21}$$

where $q_x^2(t), q_y^2(t)$ are the x, y coordinates of $\boldsymbol{q}$. Of the two s quadratic equation solutions, the smaller t value is the desired one since the ray is oriented from the source to the detector and the new virtual source position is $\mathbf{s}' = \boldsymbol{q}(t_{so})$. Then:

$$\phi' = Az(\boldsymbol{q}(t_{so})) \text{ and } h' = q_z(t_{so}). \tag{22}$$

where $\mathrm{Az}(\mathbf{k}) = \mathrm{atan2}(k_y, k_x)$ is the quadrant-aware tangent function of vector $\mathbf{k} = (k_y, k_x, k_z)$. To obtain the detector coordinates, define $\boldsymbol{w}(t) = \boldsymbol{q}(t) - \mathbf{s}'$ and note that $\boldsymbol{w}(t)$ intersects the cylinder of detector positions when $t = t_{sd}$:

$$t_{sd} = \max\left\{t : w_x^2(t) + w_y^2(t) = D_{sd}^2\right\}. \tag{23}$$

The larger solution value of t in Eq. (22) yields the new detector position $\mathbf{d}' = \boldsymbol{q}(t_{sd})$ since the ray is oriented towards the detector. The new detector coordinates are:

$$\gamma' = \phi' - Az(\boldsymbol{w}(t_{sd})) \text{ and } \upsilon' = w_z(t_{so}). \tag{24}$$

Eqs.(21), (23) define a transformation $(\phi, \gamma, \upsilon, h) \rightarrow (\phi', \gamma', \upsilon', h')$. $\tilde{\mathcal{T}}_{r,\theta,\mathbf{\Delta}}$ is obtained by substituting $h = 0$. We define a cost function for 3D cone-beam similarity as follows. Let the two scans be $\boldsymbol{\mathcal{R}}^{CB}\{f\}(\phi, \gamma, \upsilon)$ with the reconstructed f and $\boldsymbol{\mathcal{R}}^{FB}\{g\}(\phi, \gamma, \upsilon)$ with source positions $\phi \in \{\phi_1, \ldots, \phi_K\}$. The new cone-beam transform $\boldsymbol{\mathcal{R}}^{CB*}\{f\}(\phi, \gamma, \upsilon, h)$ is computed from f for $h \in \{h_1, \ldots, h_L\}$ by forward cone-beam projection. The similarity cost function is based on the normalized cross correlations between $\boldsymbol{\mathcal{R}}^{FB}\{g\}(\phi_i, \cdot, \cdot)$, the 2D projection of g from a single source position ϕ_i and $\tilde{\mathcal{T}}_{r,\theta,\mathbf{\Delta}}\{\boldsymbol{\mathcal{R}}^{CB*}\{f\}\}(\phi_i, \cdot, \cdot)$, the projection of f for ϕ_i with parameters $r, \theta, \mathbf{\Delta}$:

$$\begin{aligned} &\mathcal{C}(r, \theta, \mathbf{\Delta}) \\ &= \sum_{i=1}^{K} \log\left(1 - NCC\left[\tilde{\mathcal{T}}_{r,\theta,\mathbf{\Delta}}\left\{\boldsymbol{\mathcal{R}}^{CB*}\{f\}\right\}(\phi_i, \cdot, \cdot), \right.\right. \\ &\qquad \left.\left. \boldsymbol{\mathcal{R}}^{CB}\{g\}(\phi_i, \cdot, \cdot)\right]\right). \end{aligned} \tag{25}$$

The rigid registration is iteratively computed in 6D parameter space. It starts from an initial guess and moves towards a lower-cost solution until a local optimum is found, which is achieved when all views of $\boldsymbol{\mathcal{R}}^{CB}\{g\}$ have a high cross-correlation similarity with the resulting $\tilde{\mathcal{T}}_{r,\theta,\mathbf{\Delta}}\{\boldsymbol{\mathcal{R}}^{CB*}\{f\}\}$.

The cone-beam rigid registration algorithm inputs a sparse scan $\boldsymbol{\mathcal{R}}^{CB}\{g\}$, a dense scan $\boldsymbol{\mathcal{R}}^{CB*}\{f\}$, and an initial guess. The sampling of $\boldsymbol{\mathcal{R}}^{CB*}\{f\}$ is dense in viewing angles ϕ and source position offset h so that the interpolation with transformation $\tilde{\mathcal{T}}_{r,\theta,\mathbf{\Delta}}$ provides sufficiently accurate values for estimating the 2D correlation with $\boldsymbol{\mathcal{R}}^{CB}\{g\}$. The transformation parameters are computed by minimizing C over the 6D space of $(\boldsymbol{r}, \theta, \mathbf{\Delta})$ by derivative-free optimization, e.g., downhill simplex:

$$\left(\hat{\boldsymbol{r}}, \hat{\theta}, \hat{\mathbf{\Delta}}\right) = \min_{\mathbf{r},\theta,\mathbf{\Delta}} C(\boldsymbol{r}, \theta, \mathbf{\Delta}). \tag{26}$$

The algorithm is summarized in Table II.

TABLE II
GENERAL FRAMEWORK FOR 3D CONE-BEAM RIGID REGISTRATION

Input	• Baseline scan $\boldsymbol{\mathcal{R}}^{CB}\{f\}$, densely sampled in the view angle ϕ and detector coordinates u, v • Repeat scan $\boldsymbol{\mathcal{R}}^{CB}\{g\}$, sparsely sampled in the view angle ϕ, and densely in detector coordinates u, v
	1. Re-project the reconstructed image f to calculate a dense sampling of $\boldsymbol{\mathcal{R}}^{CB*}\{f\}$ in ϕ, h, u, v 2. Initialize $(\boldsymbol{r}, \theta, \mathbf{\Delta})$ with initial guess, or $\mathbf{0}$ (identity transformation) 3. Repeat until convergence: 3.1. Evaluate the cost function $\mathcal{C}$ for different perturbations of $(\boldsymbol{r}, \theta, \mathbf{\Delta})$ 3.2. Select the perturbation leading to largest reduction in $\mathcal{C}$ and update $(\boldsymbol{r}, \theta, \mathbf{\Delta})$ 3.3. If change below ε, return $(\boldsymbol{r}, \theta, \mathbf{\Delta})$
Output	Rigid registration which best aligns f and g: $g(X) \cong f(A_{r,\theta}X + \mathbf{\Delta})$

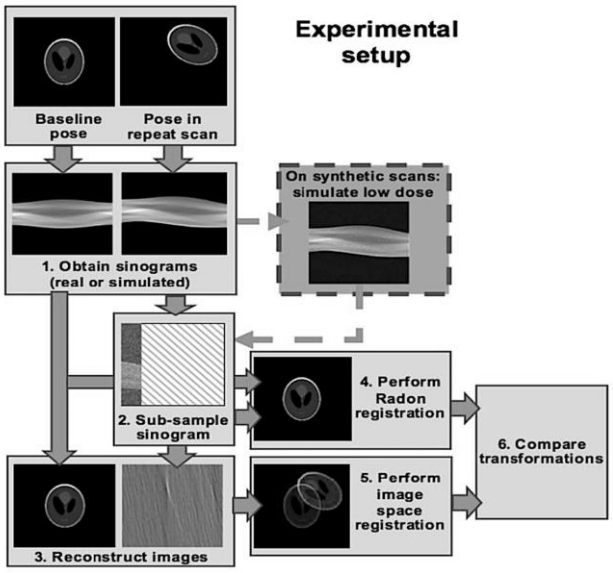

Fig. 4. Flow diagram of the steps of the two validation studies.

IV. EXPERIMENTAL STUDIES

We evaluate our method with two studies. The first study evaluates the performance of Radon registration on simulated parallel (3D) and fan-beam (2D) scan data on the Shepp-Logan phantom [26]. The second study evaluates 3D parallel beam Radon registration on real CT scan data of two phantoms and on a patient CT dataset.

A. Methodology

Fig. 4 shows the studies flow diagram. In each study, we applied a series of known rigid transformations to the baseline

image f to generate a new set of images, H. These transformations served as the ground truth. We computed the Radon transform (sinogram) of the baseline scan and of each of the transformed images $h \in H$, yielding $\mathcal{R}f$ and $\mathcal{R}h$ (step 1). We then sub-sampled the sinogram of each transformed image to produce a sparse sinogram (step 2). We generated a sparsely sampled version h' of each image in H, (step 3) with Matlab's filtered back-projection **iradon** function with a ramp filter. These images showed reconstruction artifacts.

For each sparsely sampled sinogram $\mathcal{R}h'$, we performed Radon registration with the baseline sinogram $\mathcal{R}f$ (step 4). For comparison, we performed image space registration with the Matlab **imregtform** function on each reconstructed image $h' \in H'$ with the baseline image f (step 5). The optimization in **imregtform** was gradient descent with the mean squares metric. We also tested the Elastix image-space registration with adaptive gradient descent and Mattes mutual information [27]. Since the results were poorer,we chose **imregtform** as the standard for image-based registration.

We compared the computed transformations with the ground truth transformation of f using the RMS error between pixel/voxel coordinates (step 6). The registration RMS of the real scans is reported in millimeters. For the synthetic Shepp-Logan phantom datasets, the RMS is reported in pixels as the voxel physical size is not available. We use the RMS difference as the success measure of our method: we consider an RMS error that exceeds 5 pixels/5 mm as one group of results which are not clinically usable, an RMS error of less than 2 pixels/2 mm as another group which is usable for most clinical application, and results with RMS error between 2-5 pixels/mm as suitable for a limited set of clinical applications.

We quantified the effect of four different parameters. First,we tested the robustness of Radon registration by applying rigid transformations of different magnitudes to the baseline image, simulating different repeat scan poses and measured the accuracy and convergence range of Radon registration.

Second, we measured the impact of the scanning rate and range of the sub-sampled sinogram. We used various sampling rates to uniformly sub-sample the Radon transform of there peat scan. Additionally, sinogram views were taken from angular ranges $[0°, k]$ for various values of k (Fig. 5, middle row).

Third, we tested the sensitivity of Radon registration to noise from low-dose scanning (Fig. 4, dashed box). We simulated reduced X-ray tube current effect with the noise model of [28].

B. Simulation Study

We performed both 2D and 3D parallel-beam registration simulations on the Shepp-Logan phantom as follows.

2D parallel beam registration: the performance of 2D Radon registration was tested on 2D images of the Shepp-Logan head phantom. When computing the 2D transformation, the rotation angle was computed by majority vote instead of RANSAC (Table I, step 2c). The phantom size was 128×128 pixels, zero-padded with 50 pixels in each direction. Both registration methods run in under 1 sec. Fig. 6 shows the results.

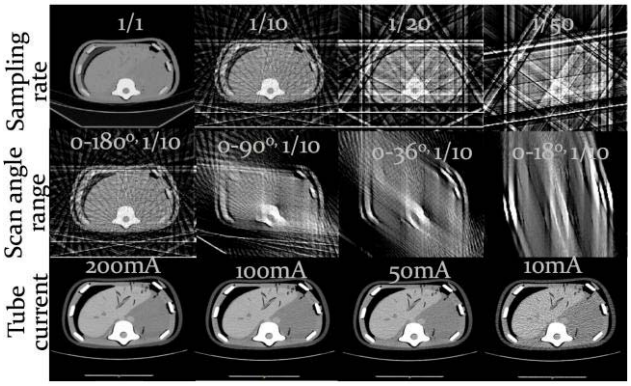

Fig. 5. Artifacts introduced in the reconstructed abdomen phantom by reducing the radiation dose in different ways. Top: decreasing sampling rates from 1/1 to 1/50 (left to right). Middle: increasingly limited scan angle range with a sampling rate of 1/10, from a full range of 180° to a range of 18°. Bottom: reducing the tube current from 200 mA (left) to 10 mA (right).

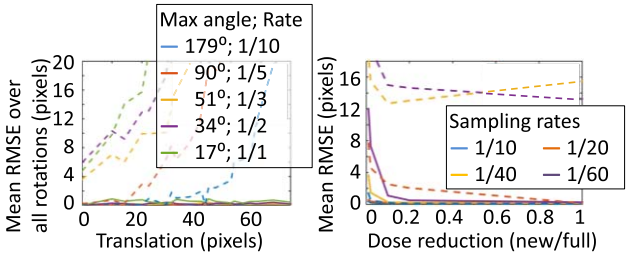

Fig. 6. Mean error of 2D Radon registration (solid lines) and image space registration (dashed lines) in simulations on Shepp-Logan head phantom. Left: large translations (horizontal axis, pixels) and limited scanning angle intervals with 18 scan angles; right: low dose (horizontal axis, dose fraction) and low sampling rates (1/10, 1/20, 1/40 and 1/60) with small transformations.

Robustness: the rigid transformations included translations ranging from −50 to 50 pixels along each axis, and rotation ranging from −50 to 50°. The sparse sinograms were obtained by sub-sampling at $1/10^{\text{th}}$ the transformed phantom sinogram. Radon registration accuracy was unaffected by the size of both the rotation and the translation, with a mean RMS error of 0.11 ± 0.05 pixels for all transformations. Image space registration produced accurate results for smaller translations,and partially failed (error >2 pixels) in 11.8% of the cases.

Scanning rate and range: we repeated the procedure above for sampling rates from 1/20 to 1/40 and for angular ranges in $[0°, k]$, for $k = 17, 34, 51, 89°$. The Radon registration accuracy was only slightly affected by the limited scanning rate and range. The mean error increased by up to 0.5 pixels, and remained <1 pixel, even when the number of angles in the sparse sinogram was 5 instead of 180, or when limiting their range to 17°. In comparison, the image space registration performance quickly plummeted: it failed in 30.6% of cases with a sampling rate of 1/20 and failed in 46.1% of cases with scanning angle range of 90° (Fig. 6, left).

Dose: the simulated doses ranged from a full dose (100%) to 1% of a full dose. The dose reduction was tested on large transformations (translations of 30-50 pixels and rotations of 40°-50°) and small transformations (translations of 10-30 pixels and rotations of 5-15°). The effects of the noise

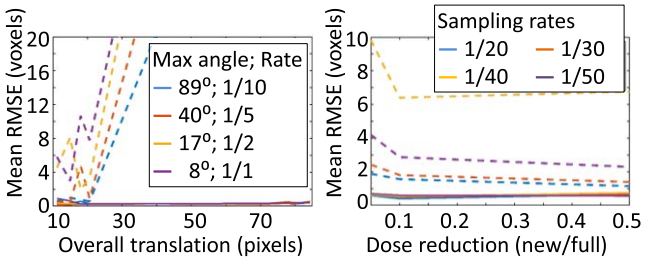

Fig. 7. Mean error of 3D Radon registration (solid lines) and image space registration (dashed lines) in simulations on 3D Shepp-Logan head phantom: left - effect of large translations (horizontal axis, pixels) and limited scanning angles intervals; right - low dose (horizontal axis, dose fraction) and low sampling rates (1/20, 1/30, 1/40 and 1/50). Radon registration is less sensitive to the transformations size, angle range, sampling rate, and dose and significantly outperforms image registration in nearly all cases.

and the scan angles choice was tested by sub-sampling the repeat scan sinogram with various sampling rates and ranges. Each condition was repeated 30 times with different random noise. Both methods proved resilient to small dose reductions, but showed a decrease in performance for <10% of the full dose (Fig. 6, right). As the dose is lowered, the effects of the sampling rate and range became more pronounced. Radon registration achieved sub-pixel accuracy with 10% dose and 5 projection angles (1/40 sampling rate) even for large transformations.

*3D parallel beam registration:*Similar experiments were run using 3D Radon registration on the 3D Shepp-Logan head phantom. Fig. 7 shows the results.

Robustness: the convergence range was evaluated with 162 transformations. The translations ranged from −50 to 50 voxels along different axes. The rotation ranged from 1.5° to 14° around the $y$axis, and from 4.7° to 42.8° around the z axis. Each test was repeated 5 times to account for the RANSAC variability (Table I, step 2c). The sparse sinogram was obtained using a sampling rate of 1/20 for both azimuth and elevation. Radon registration again proved insensitive to the transformation size, achieving sub-voxel accuracy in all cases. Image space registration was not guaranteed to converge for translations >10 voxels. Image space registration failed up to 66% of the time for large transformations.

Scanning rate and range: the azimuth angles of the sparse 3D Radon transform were sub-sampled with rates ranging from 1/20 to 1/50, or taken from intervals $[0°, k]$ for $k = 8, 17, 40, 89, 179°$. Each configuration was tested on two types of transformation: large transformations, with translations of 40-55 pixels, and small transformations, with translations of 1-15 pixels and was repeated 4 times. Radon registration again proved more robust than image space registration, with a mean error of <1.5 voxels for all sampling rates, ranges and transformation sets. The performance of image space registration was much poorer, failing at least 70% of the time with a sampling rate of 1/40 or an angle range of 17° (Fig. 7, left).

Dose: dose reductions of 50%, 10%, 5% and 1% were simulated with large and small transformations sets as above.

The elevation angles were sampled at 1/10 from a range of 90° for both the sparse and dense sinograms. The tests were run with the same sampling rates and ranges as in the previous experiment. Radon registration was only mildly affected by the dose reduction, and showed a substantial decrease in performance only for the smallest dose (1% of a full dose). With >10% of the dose, it always converged with a mean error <1.5 voxels; with 5% of a full dose it converged over 95% of the timefor both transformation sets and for all sampling rates and angle ranges > 8°. For small transformations, the performance of image space registration began degrading with a dose of 5% of a full dose (Fig. 7, right). For large transformations image space registration failed in all cases, regardless of dose.

2D fan-beam registration: We used the same Shepp-Logan phantom as above. The fan beam rotation was 1° with sensor spacing of 0.25 pixels. The source to the center of rotation distance was 342 pixels.

Robustness: the convergence rate was evaluated for 1,080 transformations, consisting of rotations of up to 50° and translations of up to 50 pixels along each axis. The scan angles were sampled at a rate of 1/20. Each test was repeated 5 times to account for the algorithm's random choices.Radon registration yielded sub-pixel accuracy for translations <30 pixels and rotation < 40°. With rotations < 10°, sub-pixel accuracy wasachieved with translations of up to 50 pixels.

*Scanning rate and range:*we tested the effect of sampling rates ranging from 1/10 to 1/60 and angular ranges in $[0°,k]$ intervals, for $k = 17, 89, 179°$, with large transformations (translations of 30-50 pixels and rotations of 40°-50°) and small transformations (translations of 0-30 pixels and rotations of 0°-15°). Each test was repeated 5 times. Fan beam Radon registration succeeded in >99% of cases for sampling rates >1/40 for all angle ranges on small transformations with mean error <1 pixel for all sampling rates and angle ranges. The performance was slightly poorer for large transformations, with sub-pixel accuracy with 1/10 sampling rate or angle range of 89°. Thus, the performance of fan beam registration is comparable to parallel beam registration in Radon space.

Dose: the same procedure was repeated for dose reductions of 20%, 10%, 2% and 1%. There was a minor decrease in performance, although the mean error remained <1 pixel. This indicates similar robustness to that of parallel beam scans.

To evaluate the properties of the fan-beam cost function, we used registered 2D slices from consecutive scans of the head phantom, where one of the slices was transformed for different values of the translation and rotation parameters, and the cost was evaluated at each step (Fig. 8). The evaluation shows a minimum which is global at the selected ranges of ±50° rotation, ±50 mm translations. Though the neighborhood of the minimum is not steep, the simulations described above show subpixel accuracy was achieved.

C. Real CT scan study

We performed 3D parallel beam Radon registration on real CT scans of 3 head and abdomen phantoms and on a clinical patient CT (Figs. 9 and 10). Table III summarizes the datasets used in the study.

*Phantom scans:*Two CT scan datasets were acquired with a GE Discovery CT750HD scanner (General Electric). Dataset

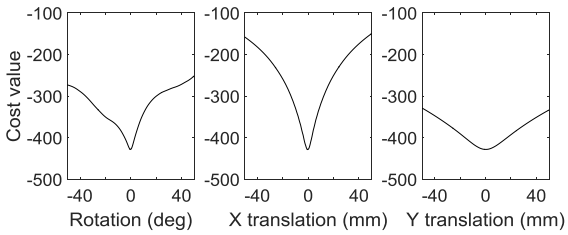

Fig. 8. Fan beam cost function investigation. The cost is shown for different transformations involving rotation only, translation in the x direction only, and translation in the y direction only. The plots were produced using a pair of registered slices from the head phantom dataset.

TABLE III
DATASETS USED IN VALIDATION STUDIES

	Dataset	Sinogram acquisition	Tube currents	Comments
1	Head phantom	GE Discovery CT750HD	200mA, 10mA	See Fig. 9, 10
2	Abdomen phantom	GE Discovery CT750HD	200mA, 10mA	
3	Patient scan	Reprojected from images	Not disclosed	See Fig. 12

Fig. 9. Head (left) and abdomen phantom (center), actual CT scan (right).

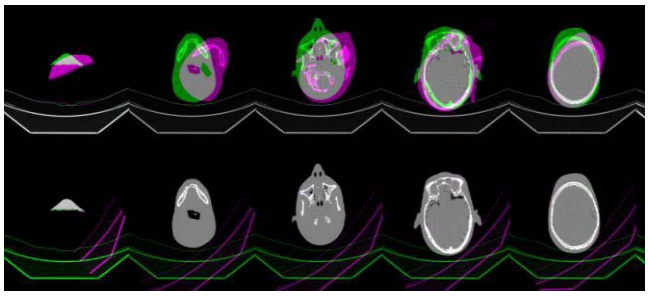

Fig. 10. Overlay of 5 representative slices from two CT scans of the head phantom: before (top) and after 3D Radon space registration (bottom).

1 images are $600 \times 600 \times 220$ voxels; Dataset 2 images are $600 \times 600 \times 120$ voxels, all $0.58 \times 0.58 \times 1.25\text{mm}^3$.The raw sinogram data consisted of 855 detectors of width 0.58 mm with 984 views of 0.36° angular resolution. Dataset 1 includes a baseline scan of the head phantom acquired at 200 mA and five repeat scans in different poses acquired at 10 mA. Dataset 2 consists of two scans of the abdomen phantom acquired at 10 mA and 200 mA. The transformations between the baseline and repeat scan phantom positions include translations of up to 47 mm and rotations of up to 35° along different axes. To prevent registration bias, a full-dose scan of the empty CT scanner bed was acquired and subtracted from all images and

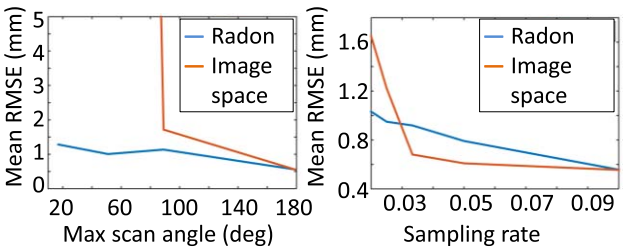

Fig. 11. Mean RMS error of 3D Radon registration (blue) and image space registration (red) in simulations on the GE head phantom with different transformations: Left - limited scan angle ranges, right - limited sampling rates. Radon outperforms image space for limited scan angles and is comparable to image space registration for low sampling rates.

their sinograms. Radon registration required 1-2 mins, while image space registration required 5-20 mins.

Registration was first performed on Dataset 1. The inputs were the raw sinogram from the CT scanner. The ground truth was obtained by image space registration on the full dose scans. We tested the effect of the scanning rate and range for the low dose repeat scan.

Scanning rate and range: the azimuth angles of the sparse 3D Radon transform were sub-sampled with 1/10-1/50 rates, or in intervals $[0°,k]$, $k = 17,51,89,179°$. Radon registration only failed (>2 mm) in the most difficult experiment conditions–20% of the time with 1/50 sampling rate or 17° angle range. Image space registration succeeded with a sampling rate of 1/30 or a full angle range. Its failure rate ranged from 20% (1/40 sampling rate) to 100% (angle range of 17°). The mean error of both methods was comparable for all sampling rates (Fig. 11).

To test a wider range of transformations without acquiring new CT scans, we applied known transformations to the low dose scan from Dataset 2, with the original scan as the baseline and the transformed images as the repeat scans. We synthetically generated sinograms from these images.

Robustness: we tested three scenarios: small transformations (1-20 mm translation and 1-10° rotation along any axis), large rotations (15°-35°), and large translations (29-65 mm). Each set consisted of 16 transformations. In both sinograms, the elevations were sampled 1/10 in the range [0°, 90°]. In the sparse sinogram, the azimuth was also sampled at 1/10. Both registration methods converged for all transformations.

Scanning rate and range: the experiments were repeated with sampling rate of 1/50 and with a range of 51°. In both cases, Radon registration succeeded 100% with a mean error <1.2 mm. Image space registration failed 100% with a limited scan angle range, regardless of the transformation. With a low sampling rate, the overall failure rate was 35.4%.

Dose: the same procedure was repeated using the scan acquired at 200 mA. Overall, the results were similar to those reported above, with the exception of the lowered sampling rate condition. With a higher dose, image space registration performed somewhat better, with a failure rate of 22.9%.

Real patient scans: we tested our method on a pair of CT scans of a patient head taken at two different times of size $0.42 \times 0.42 \times 0.67\text{mm}^3$ each (Fig. 12, left). The sinograms were artificially recreated, as only the reconstructed images

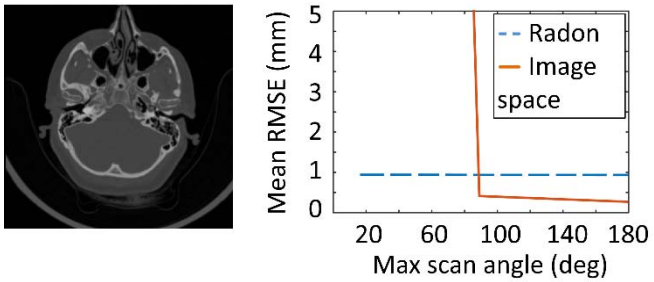

Fig. 12. Patient CT dataset and mean RMS error of 3D Radon registration (blue) and image space registration (red) for limited angle ranges.

were available. Prior to re-projection, the CT scanner bed was removed from both images and the ground-truth transformation was computed by image-based registration. We repeated the procedure used for the phantom scan experiments, comparing the effect of the sampling rate and scan angle range on image-based registration and on our method. (Fig. 12, right). The RMSE of our method was <1 mm for all cases. As in the previous experiments, image-based registration succeeded for small sampling rates but failed for angle ranges $< 90°$ because the sparsely sampled image is very different than the fully sampled image (Fig. 5, middlerow, scan angle range $> 90°$). This indicates that our method yields results comparable to full-resolution image-space registration with about 10% of the radiation dose of the second scan.

V. Discussion

We conclude that sparse 3D Radon registration is highly robust, insensitive to the repeat scan pose, the scanning rate and range, the field-of-view, and the dose. The results are consistent for both synthetic data scans and real scans. In particular, our method: 1) out-performs image space registration under similar sparse sampling conditions; 2) supports much larger transformations than image space registration (translations >50 mm); 3) always converges, even with large transformations, 5% of the dose, and a sampling rate of 1/50 or angle range of 50° for parallel-beam geometry; 4) allows for a theoretical dose reduction beyond 1/100 by combining low tube current scanning and limited scanning rate and ranges (ultralow dose scanning). This fractional scanning technique is feasible with existing hardware (personal communication, GE Healthcare CT experts, Tirat HaCarmel, Israel).

An advantage of our method over existing projection-based methods [8]–[17] is that for parallel-beam geometry, it provides a closed-form solution that decouples the rotation and translation parameters. Thus, our method does not have convergence issues and accumulated estimation errors. For fan-beam scanning, our Shepp-Logan simulation results show that the optimization has a high accuracy and success rate with sub-pixel mean coordinate error in over 99% of tested transformations, and has a good convergence range of up to 30 pixels translation and 50° rotation. Note that the NCC measure and RANSAC in the matching step can be replaced by other alternatives.

Study limitations: First, the scope of the study is limited since the real phantom datasets were specifically acquired for the study, the number of setups was relatively small. Furthermore, the unknown ground truth transformation was computed using image space registration, which may skew the results in favor of it. We partially compensated for this by testing a larger numbers of transformations on the synthetic datasets and by applying transformations to the real scans. As expected, the results for synthetic data were better than those for real scans, although the observed pattern is similar. Second, the number of synthetic 3D configurations that were tested was limited by the run time of the image space registration method: 5-20 mins vs. 1-2 min for Radon space registration. Third, no changes in the images were considered. However, initial experiments suggest that that small changes only mildly reduce the Radon registration performance.

Method limitations: Our methods are limited to rigid registration. However, rigid registration is an important first step for non-rigid registration to bring the datasets into coarse correspondence. It also increases the convergence range and improves computation time. The concept of sparse repeat CT sampling may be extended to deformable registration with ana-priori deformation model, i.e., patient breathing.

An issue is how to achieve repeat scanning dose reduction in existing CT scanners. Dose reduction can be achieved by: 1) full-range low dose scanning; 2) on-line fractional scanning.

Our experiments indicate that 3D Radon registration can be performed with the lowest possible dose (10-20 mA) without compromising robustness and accuracy. This results in a tenfold dose radiation reduction with respect to a full dose scan.

On-line fractional scanning consists of limiting the angular CT scanning range to intervals during scanning. Fractional scanning in a small range of few tenths of degrees is achievable with existing software and hardware by tube potential switching and tube current modulation. For example, tube current modulation is used in snapshot heart scanning to acquire 2-4 angular views in 2-4 adjacent heart cycles. Dual-voltage CT scanners switch the tube voltage between higher voltage (140 kV) to lower voltage (80 kV) every 1°. By alternatively switching the voltage to 80-100 kV and 30-40 kV (where the harmful absorbed radiation is extremely low) for a wider angular range of $10° \sim 20°$, an X-ray dose reduction of $\times$10-50 can be achieved. Other dose reduction methods include *xy* plane tube current modulation and active collimation [23].

Clinical relevance: We conjecture that our method can be used to replace fiducial-based registration by obviating the need to reconstruct the repeat scan and locate the registration fiducials in the baseline and repeat scan images. It can also replace 2D X-ray based methods by providing a fully automatic on-site patient registration method in the CT scanner that does not require additional calibration or hardware setup. It can replace image-based needle CT-guided methods when the needle can be detected in sinogram space.

VI. Conclusion

We have presented a new rigid registration method for CT scans in 3D Radon space. Its key characteristic is that it allows the registration of a full-resolution CT scan to a

sparsely-sampled CT scan without compromising the registration accuracy. This results in a significant X-ray dose reduction when registering a diagnostic CT scan to the patient during interventional CT procedures. Our results show that a very small number of scan directions yield voxel size accuracy with a wide convergence range. Radon-space registration has the potential to perform patient-to-CT registration with the lowest possible dose, below that of any other image-based methods since very few scanning rays/directions are required, as shown here.Since the method is automatic and can be performed with the same hardware, it supports frequent ultralow dose scanning to track the patient and the surgical instruments.

REFERENCES

[1] E. J. Hall and D. J. Brenner, "Cancer risks from diagnostic radiology," *Brit. Inst. Radiol.*, vol. 81, no. 965, pp. 362–378, Feb. 2008.

[2] F. A. Mettler, Jr., P. W. Wiest, J. A. Locken, and C. A. Kelsey, "CT scanning: Patterns of use and dose," *J. Radiol. Protection*, vol. 20, no. 4, p. 353, 2000.

[3] P. J. Besl and N. D. McKay, "A method for registration of 3D shapes," *IEEE Trans. Pattern Anal. Mach. Intell.*, vol. 14, no. 2, pp. 239–256, Feb. 1992.

[4] J. B. A. Mainz and M. A. Viergever, "A survey of medical image registration," *Med. Image Anal.*, vol. 2, no. 1, pp. 1–36, Mar. 1998.

[5] M. W. K. Kan, L. H. T. Leung, W. Wong, and N. Lam, "Radiation dose from cone beam computed tomography for image-guided radiation therapy," *Int. J. Radiat. Oncol.*, vol. 70, no. 1, pp. 272–279, Jan. 2008.

[6] P. Markelja, D. Tomaževič, B. Likar, and F. Pernus, "A review of 3D/2D registration methods for image-guided interventions," *Med. Image Anal.*, vol. 16, no. 3, pp. 642–661, Apr. 2012.

[7] Y. Otake *et al.*, "Intraoperative image-based multiview 2D/3D registration for image-guided orthopaedic surgery: Incorporation of fiducial-based C-arm tracking and GPU-acceleration," *IEEE Trans. Med. Imag.*, vol. 31, no. 4, pp. 948–961, Apr. 2012.

[8] A. Khamene, R. Chisu, W. Wein, N. Navab, and F. Sauer, "A novel projection based approach for medical image registration," in *Biomedical Image Registration*, vol. 4057. New York, NY, USA: Springer-Verlag, 2006, pp. 247–256.

[9] M. Freiman, O. Pele, A. Hurvitz, M. Werman, and L. Joskowicz, "Spectral-based 2D/3D X-ray to CT image rigid registration," *Proc. SPIE*, vol. 7964, p. 79641B, Mar. 2011.

[10] W. Mao, T. Li, N. Wink, and L. Xing, "CT image registration in sinogram space," *Med. Phys.*, vol. 34, no. 9, pp. 3596–3602, Sep. 2007.

[11] R. Mooser, F. Forsberg, E. Hack, G. U. Székely, and U. Sennhauser, "Estimation of affine transformations directly from tomographic projections in two and three dimensions," *Mach. Vis. Appl.*, vol. 24, no. 2, pp. 419–434, Feb. 2013.

[12] J. You, W. Lu, J. Li, G. Gindi, and Z. Liang, "Image matching for translation, rotation and uniform scaling by the Radon transform," in *Proc. Int. Conf. Image Process. (ICIP)*, Oct. 1998, pp. 847–851.

[13] W. Lu *et al.*, "Image/patient registration from (partial) projection data by the Fourier phase matching method," *Phys. Med. Biol.*, vol. 44, no. 8, p. 2029, Aug. 1999.

[14] E. E. Fitchard, J. S. Aldridge, P. J. Reckwerdt, and T. R. Mackie, "Registration of synthetic tomographic projection data sets using cross-correlation," *Phys. Med. Biol.*, vol. 43, no. 6, p. 1645, Jun. 1998.

[15] E. E. Fitchard, J. S. Aldridge, P. J. Reckwerdt, G. H. Olivera, T. R. Mackie, and A. Iosevic, "Six parameter patient registration directly from projection data," *Nucl. Instrum. Methods Phys. Res. A, Accel., Spectrometers, Detect. Assoc. Equip.*, vol. 421, nos. 1–2, pp. 342–351, Jan. 1999.

[16] W. Wein and A. Ladiko, "Detecting patient motion in projection space for cone-beam computed tomography," in *Medical Image Computing and Computer-Assisted Intervention*, Sep. 2011, pp. 516–523.

[17] A. Aichert *et al.*, "Redundancies in X-ray images due to the epipolar geometry for transmission imaging," in *Proc. 3rd Int. Conf. Image Formation X-Ray Comput. Tomogr.*, 2014, pp. 333–337.

[18] A. Aichert *et al.*, "Epipolar consistency in transmission imaging," *IEEE Trans. Med. Imag.*, vol. 34, no. 11, pp. 2205–2219, Nov. 2015.

[19] A. R. Osorio, R. A. Isoardi, and G. Mato, "Non-rigid registration of tomographic images with Fourier transforms," *J. Phys., Conf. Ser.*, vol. 90, no. 1, p. 012058, 2007.

[20] H. Zhang, L. Ouyang, J. Huang, J. Ma, W. Chen, and J. Wang, "Few-view cone-beam CT reconstruction with deformed prior image," *Med. Phys.*, vol. 41, no. 12, p. 121905, Dec. 2014.

[21] A. Uneri *et al.*, "Evaluation of low-dose limits in 3D-2D rigid registration for surgical guidance," *Phys. Med. Biol.*, vol. 59, no. 18, p. 5329, Aug. 2013.

[22] Y. K. Kim *et al.*, "Ultra-low-dose CT of the thorax using iterative reconstruction: Evaluation of image quality and radiation dose reduction," *Amer. J. Roentgenol.*, vol. 204, no. 6, pp. 1197–1202, Jun. 2015.

[23] T. R. Mackie, "History of tomotherapy," *Phys. Med. Biol.*, vol. 51, no. 13, p. R427, Jun. 2006.

[24] G. Medan, A. Kronman, and L. Joskowicz, "Reduced-dose patient to baseline CT rigid registration in 3D Radon space," in *Proc. Int. Conf. Med. Image Comput. Comput.-Assist. Intervent. (MICCAI)*, Sep. 2014, pp. 291–298.

[25] M. A. Fischler and R. C. Bolles, "Random sample consensus: A paradigm for model fitting with applications to image analysis and automated cartography," *Commun. ACM*, vol. 24, no. 6, pp. 381–395, Jun. 1981.

[26] L. A. Shepp and B. F. Logan, "The Fourier reconstruction of a head section," *IEEE Trans. Nucl. Sci.*, vol. 21, no. 3, pp. 21–43, Jun. 1974.

[27] S. Klein, M. Staring, K. Murphy, M. A. Viergever, and J. P. W. Pluim, "Elastix: A toolbox for intensity based medical image registration," *IEEE Trans. Med. Imag.*, vol. 29, no. 1, pp. 196–205, Jan. 2010.

[28] S. Žabić, Q. Wang, T. Morton, and K. M. Brown, "A low dose simulation tool for CT systems with energy integrating detectors," *Med. Phys.*, vol. 40, no. 3, p. 031102, Mar. 2013.

[29] N. Nacereddine, S. Tabbone, and D. Ziou, "Similarity transformation parameters recovery based on Radon transform. Application in image registration and object recognition," *Pattern Recognit.*, vol. 48, no. 7, pp. 2227–2240, Jul. 2015.

[30] Y. Wan and N. Wei, "A fast algorithm for recognizing translated, rotated, reflected, and scaled objects from only their projections," *IEEE Signal Process. Lett.*, vol. 17, no. 1, pp. 71–74, Jan. 2010.

[31] C. Debbeler, N. Maass, M. Elter, F. Dennerlein, and T. M. Buzug, "A new CT rawdata redundancy measure applied to automated misalignment correction," in *Proc. 12th Int. Meeting Fully Three-Dimensional Image Reconstruct. Radiol. Nucl. Med.*, 2013, pp. 264–267.